Journal of Nuclear Medicine, published on October 16, 2008 as doi:10.2967/jnumed.108.054015

In Vitro and In Vivo Evaluations of a Hydrophilic ^{64}Cu-Bis(Thiosemicarbazonato)–Glucose Conjugate for Hypoxia Imaging

Simon R. Bayly[1,2], Robert C. King[3], Davina J. Honess[3], Peter J. Barnard[2], Helen M. Betts[2], Jason P. Holland[2], Rebekka Hueting[2,3], Paul D. Bonnitcha[2], Jonathan R. Dilworth[1,2], Franklin I. Aigbirhio[4], and Martin Christlieb[3]

[1]Siemens Oxford Molecular Imaging Laboratory, Inorganic Chemistry Laboratory, University of Oxford, Oxford, United Kingdom; [2]Chemistry Research Laboratory, Department of Chemistry, University of Oxford, Oxford, United Kingdom; [3]CRUK/MRC, Gray Institute for Radiation Oncology and Biology, University of Oxford, Headington, Oxford, United Kingdom; and [4]The Wolfson Brain Imaging Centre, Addenbrooke's Hospital, Cambridge, United Kingdom

A water-soluble glucose conjugate of the hypoxia tracer ^{64}Cu-diacetyl-bis(N^4-methylthiosemicarbazone) (^{64}Cu-ATSM) was synthesized and radiolabeled (^{64}Cu-ATSE/A-G). Here we report our initial biological experiments with ^{64}Cu-ATSE/A-G and compare the results with those obtained for ^{64}Cu-ATSM and ^{18}F-FDG. **Methods:** The uptake of ^{64}Cu-ATSE/A-G and ^{64}Cu-ATSM into HeLa cells in vitro was investigated at a range of dissolved oxygen concentrations representing normoxia, hypoxia, and anoxia. Small-animal PET with ^{64}Cu-ATSE/A-G was performed in male BDIX rats implanted with P22 syngeneic carcinosarcomas. Images of ^{64}Cu-ATSM and ^{18}F-FDG were obtained in the same model for comparison. **Results:** ^{64}CuATSE/A-G showed oxygen concentration–dependent uptake in vitro and, under anoxic conditions, showed slightly lower levels of cellular uptake than ^{64}Cu-ATSM; uptake levels under hypoxic conditions were also lower. Whereas the normoxic uptake of ^{64}Cu-ATSM increased linearly over time, ^{64}Cu-ATSE/A-G uptake remained at low levels over the entire time course. In the PET study, ^{64}CuATSE/A-G showed good tumor uptake and a biodistribution pattern substantially different from that of each of the controls. In marked contrast to the findings for ^{64}Cu-ATSM, renal clearance and accumulation in the bladder were observed. ^{64}Cu-ATSE/A-G did not display the characteristic brain and heart uptake of ^{18}F-FDG. **Conclusion:** The in vitro cell uptake studies demonstrated that ^{64}Cu-ATSE/A-G retained hypoxia selectivity and had improved characteristics when compared with ^{64}Cu-ATSM. The in vivo PET results indicated a difference in the excretion pathways, with a shift from primarily hepatointestinal for ^{64}Cu-ATSM to partially renal with ^{64}Cu-ATSE/A-G. This finding is consistent with the hydrophilic nature of the glucose conjugate. A comparison with ^{18}F-FDG PET results revealed that ^{64}Cu-ATSE/A-G was not a surrogate for glucose metabolism. We have demonstrated that our method for the modification of Cu-bis(thiosemicarbazonato) complexes allows their biodistribution to be modified without negating their hypoxia selectivity or tumor uptake properties.

Key Words: PET; molecular imaging; ^{64}Cu-ATSM; hypoxia; biodistribution

J Nucl Med 2008; 49:1862–1868
DOI: 10.2967/jnumed.108.054015

Tumor hypoxia is an important feature of solid tumors. It is closely correlated with resistance to radiotherapy and chemotherapy (*1–3*) as well as the initiation of angiogenesis and metastasis (*4,5*), which lead to malignant progression. Because hypoxia has a profound impact on patient survival (*6*), methods for the detection and quantification of hypoxia are currently the subject of intense investigation. Several radiolabeled markers have been developed for PET imaging of hypoxia—notably, ^{18}F-fluoromisonidazole (*7–9*) and Cu-diacetyl-bis(N^4-methylthiosemicarbazone) (Cu-ATSM, where Cu is either ^{60}Cu, ^{62}Cu, or ^{64}Cu) (*10,11*). ^{60}Cu-ATSM has been shown to be predictive of radiotherapy treatment outcome in small-scale clinical studies, and ^{64}Cu-ATSM recently entered clinical trials in the United States (*12–14*). The blood clearance and excretion kinetics of Cu-ATSM are not ideal, and high levels of liver and kidney uptake have been observed. For improved hypoxia imaging, it is therefore desirable to modify the biodistribution properties of Cu-ATSM, in particular, its excretion pathway, without diminishing its ability to discriminate tumor hypoxia.

The mechanism of hypoxia selectivity of Cu-ATSM and related complexes (Fig. 1) is thought to involve an initial intracellular proton-coupled reduction to produce a copper(I) species, followed by reoxidation and efflux from cells with high oxygen tension or by ligand dissociation and trapping of the copper in cells with low oxygen tension (*15*). Dearling et al. conducted an extensive structure–activity survey of Cu-bis(thiosemicarbazonato) complexes and found that hypoxia selectivity was correlated with [**Fig. 1**]

Received May 2, 2008; revision accepted Jul. 17, 2008.
For correspondence or reprints contact: Martin Christlieb, Gray Institute for Radiation Oncology and Biology, University of Oxford, Old Road Campus Research Bldg., Old Road Campus, Headington, Oxford OX3 7DQ, United Kingdom.
E-mail: martin.christlieb@rob.ox.ac.uk

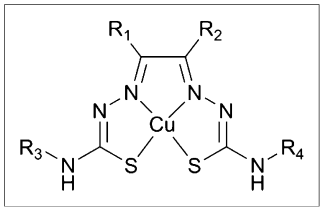

FIGURE 1. Structure of Cu-bis(thiosemicarbazonato) complexes (Cu-ATSM R_1 = R_2 = R_3 = R_4 = methyl).

the copper(II/I) redox potential as dictated by the nature of the ligand backbone (Fig. 1, R_1 and R_2) (*16,17*). We have developed methods for the synthesis of Cu-ATSM nonsymmetrically substituted at R_3 and R_4 and have shown that variations in the exocyclic amine substituents have a relatively minor influence on the redox potential of the copper(II) center (*18,19*) and should not affect hypoxia selectivity. When R_3 or R_4 is a reactive amino group (Fig. 2A), the bis(thiosemicarbazonato) core can be conjugated to a biologically active molecule, such as glucose (*19*). Glucose is of particular interest because it is hydrophilic and is avidly metabolized by many types of tumors. A Cu-ATSM–glucose derivative may also possess these properties and therefore permit improved hypoxic tumor imaging.

[**Fig. 2**]

We previously described the synthesis of Zn-ATSE/A-G (Fig. 2B) and demonstrated that copper–zinc exchange could be used to prepare the ^{64}Cu-radiolabeled compound ^{64}Cu-ATSE/A-G (Fig. 2C) (*19*). In this article, we describe the oxygen-dependent uptake of ^{64}Cu-ATSE/A-G into HeLa cells in vitro and preliminary in vivo imaging results obtained in male BDIX rats with implanted P22 syngeneic carcinosarcomas.

MATERIALS AND METHODS

Synthesis of Labeling Precursors

The proligand H_2-ATSM, Zn-ATSM, and Zn-ATSE/A-G were prepared according to published methods (*17–20*).

Preparation of ^{64}Cu-ATSE/A-G for Cell Uptake Studies and Small-Animal PET

^{64}Cu-ATSE/A-G was prepared by transmetallation of Zn-ATSE/A-G. The precursor complex (1.0 mg) was dissolved in deionized water (1.0 mL). A 50-μL sample of this solution was diluted with deionized water (200 μL), and aqueous ^{64}Cu-diacetate [^{64}Cu(OAc)$_2$] (250 μL, 20–50 MBq) was added. After 20 min of stirring at room temperature, high-performance liquid chromatography (HPLC) analysis revealed 71.7% conversion of ^{64}Cu(OAc)$_2$ (retention time, 2.62 min) to ^{64}Cu-ATSE/A-G (retention time, 9.33 min). The nonreacted ^{64}Cu(OAc)$_2$ was removed by use of a Sep-Pak (C_{18}) cartridge (Waters). The cartridge was conditioned with ethanol (5.0 mL) and deionized water (3.0 mL) before the reaction mixture was loaded. Deionized water (2.0 mL) was passed through to remove nonreacted ^{64}Cu(OAc)$_2$. ^{64}Cu-ATSE/A-G was eluted with ethanol (2 × 0.1 mL) and diluted with saline solution (0.9%, 1.8 mL) for use in PET experiments. The radiochemical purity of the administered ^{64}Cu-ATSE/A-G was greater than 95%, with specific activity in the range of 10–40 MBq/mL (or 0.2–0.8 MBq/μg of Zn-ATSE/A-G).

Preparation of ^{64}Cu-ATSM for Cell Uptake Studies and Small-Animal PET

Samples for small-animal PET were prepared by 2 different methods: by labeling of the bis(thiosemicarbazone) proligand H_2-ATSM (*15*) and by transmetallation of Zn-ATSM. A dimethyl sulfoxide solution of Zn-ATSM or H_2-ATSM (50 μL, 1.0 mg/mL) was diluted with deionized water (200 μL), and aqueous ^{64}Cu(OAc)$_2$ (250 μL, 20–50 MBq) was added. After 10 min of stirring at room temperature, the samples were purified by use of a Sep-Pak cartridge as described earlier. The radiopharmaceutical was formulated in a solution of 10% ethanol and saline (1.0 mL). Radio-HPLC results were identical for samples produced by either method. Mixtures spiked with isolated cold Cu-ATSM confirmed the identity of the radio-HPLC peak as ^{64}Cu-ATSM. The radiochemical purity of the administered radiopharmaceutical was greater than 98%, with specific activity in the range of 10–40 MBq/mL (or 0.2–0.8 MBq/μg of precursor).

Serum Stability

A 1.0 mM solution of cold Cu-ATSE/A-G (200 μL) was prepared as previously described (*19*). This solution was added to rat serum (500 μL; Sigma-Aldrich) maintained at 37°C in a water bath. Immediately after mixing of the solution, a 200-μL sample was withdrawn and added to water (1.5 mL) in a UV/visible-light cuvette. The absorption spectrum of the solution was measured with a Perkin-Elmer Lamda 19 UV/visible-light spectrometer. A cuvette containing the same concentration of serum in water (also kept at 37°C) was used as a background reference. Further samples were withdrawn at 30 and 60 min, and their spectra were measured in the same way. The absorptivity of the solution at 460 nm was assumed to be proportional to the concentration of intact Cu-ATSE/A-G in the solution.

Cell Uptake Studies

For radiotracer uptake experiments, suspensions of HeLa cells (5 mL of 10^6 cells/mL) were incubated in glass vessels in a humidified atmosphere under anoxic, hypoxic, or normoxic conditions with 5% CO_2 and the balance N_2 (with a constant flow of gas) at 37°C. The medium used was minimum essential medium with the Eagle–Spinner modification (Earle's salts and sodium bicarbonate), without calcium chloride and L-glutamine, and supplemented with L-glutamine (0.292 g/L), penicillin–streptomycin, and nonessential amino acids. After 1 h, the oxygen conditions had reached equilibrium (probed with an Oxford Optronics Oxylab pO_2 tissue oxygenation monitor), and

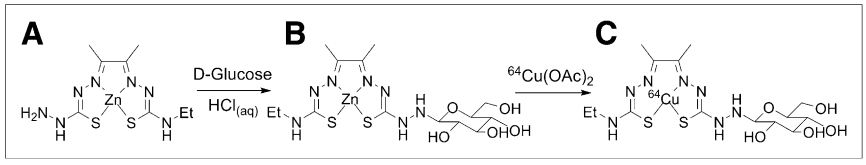

FIGURE 2. Synthesis of ^{64}Cu-ATSM derivatives. (A) Zn-ATSE/A. (B) Zn-ATSE/A-G. (C) ^{64}Cu-ATSE/A-G.

jnm054015-pe ■ 10/10/08

the N_2-purged radiotracer was added. Samples (1 mL) were taken by use of a long needle syringe at 5, 15, 30, 45, and 60 min, and three 300-μL portions of each sample were dispensed into Eppendorf tubes. The tubes were spun to pellet the cells, and the supernatant liquid was removed. The activities of the cell pellet and of the supernatant liquid were measured with a Perkin–Elmer Wizard 1470 automatic γ-counter. The uptake of ^{64}Cu as a percentage of the activity injected was calculated and plotted. A control experiment was performed with the radiotracer in minimum essential medium under normoxic conditions to assess the amount of ^{64}Cu adhering to the plastic Eppendorf tubes; this value was measured and subtracted from each data point.

Small-Animal PET

Early-generation transplants of P22 syngeneic carcinosarcomas were used for all experiments (*21*). The tumors were grown subcutaneously on the left flank of 7- to 9-wk-old male BDIX rats. Rats were used in the imaging experiments at approximately 14–21 d after implantation, when the tumors were between 1.5 and 2.0 cm in maximum diameter. The animals were treated according to protocols approved by the U.K. Home Office and the local ethics committee, in accordance with the U.K. Animals (Scientific Procedures) Act of 1986. ^{64}Cu tracers were produced as described earlier with $^{64}CuCl_2$ provided by The Wolfson Brain Imaging Centre. ^{18}F-FDG was purchased from PETNET Solutions Ltd.

The rats were anesthetized with halothane–oxygen vapor and then injected intraperitoneally with fentanyl–fluanisone and midazolam. A tail vein and a tail artery were cannulated to permit the intravenous administration of the tracer and to monitor mean arterial blood pressure, respectively. Rats were kept warm in the prone position on a custom-made cradle with an electrically warmed mat fitted with feedback control from a rectal probe. Images were acquired (Concorde microPET 220) (*22*) beginning with the injection of the tracer. The scanner field of view is approximately 80 mm long; therefore, multiple bed positions were required to image an entire animal, excluding the tail. Images were acquired at 3 different bed positions corresponding to the head (at 0–20 min and 60–80 min), the middle section (at 20–40 min and 80–100 min), and the rear section (at 40–60 min and 100–120 min). The bed positions were chosen to ensure a small amount of overlap between images. The images were connected (incorporating a decay correction) by use of Asipro software (Siemens). Transmission scans were obtained with a sealed ^{57}Co point source to correct for attenuation of the 511-keV photons. At the completion of image acquisition, the rats were euthanized by intravenous injection of pentobarbital sodium (Euthatal; Merial Animal Health Ltd.).

Calculation of Standardized Uptake Values (SUVs) and Statistical Analysis

The PET projection data (list-mode data) were binned to 23 time frames: 5 × 10 s, 7 × 15 s, 10 × 30 s, and 1 × 300 s. Regions of interest were defined by use of Inveon Research Workplace software (Siemens) to paint the entire tissue, except for intestinal tissue, in which only the main regions of activity were characterized, and muscle tissue, which was sampled by painting a region within the right thigh muscle. The SUV was measured as the decay-corrected radiotracer concentration normalized to the injected dose and animal weight. SUVs were obtained at 18 min for the brain; at 32 min for the liver, intestine, left and right kidneys, and heart; and at 42 min for the tumor, bladder, and muscle. Different time points were required for each set of organs because of the acquisition time for the relevant portion of the animal. When the activity observed was too low for an organ to be delineated, the SUV was recorded as 0. For comparison of the differences in cell uptake and SUVs, the Student t test was performed. Differences at the 95% confidence level ($P < 0.05$) were considered significant.

RESULTS

In Vitro Uptake into HeLa Cells

HeLa cells were equilibrated at 21%, 0.5%, and 0% oxygen concentrations, and the uptake of ^{64}Cu-ATSE/A-G was measured in triplicate at 5, 15, 30, 45, and 60 min after addition (Fig. 3A). After 5 min, the percentages of uptake were similar (~8.5%) for all oxygen concentrations. Under normoxic (21% O_2) conditions, uptake rose to 9.7% at 30 min and remained at the same level for the remaining 30 min. Under hypoxic (0.5% O_2) conditions, uptake increased linearly over the entire time course to reach 22.5% at 60 min. Cell uptake under anoxic (0% O_2) conditions also increased, but more steeply, to reach 30.4% at 60 min. Thus, the level of uptake of ^{64}Cu-ATSE/A-G in the HeLa cell line was strongly dependent on the O_2 concentration, and the ratio of hypoxic uptake to normoxic uptake at 60 min was 2.3. [**Fig. 3**]

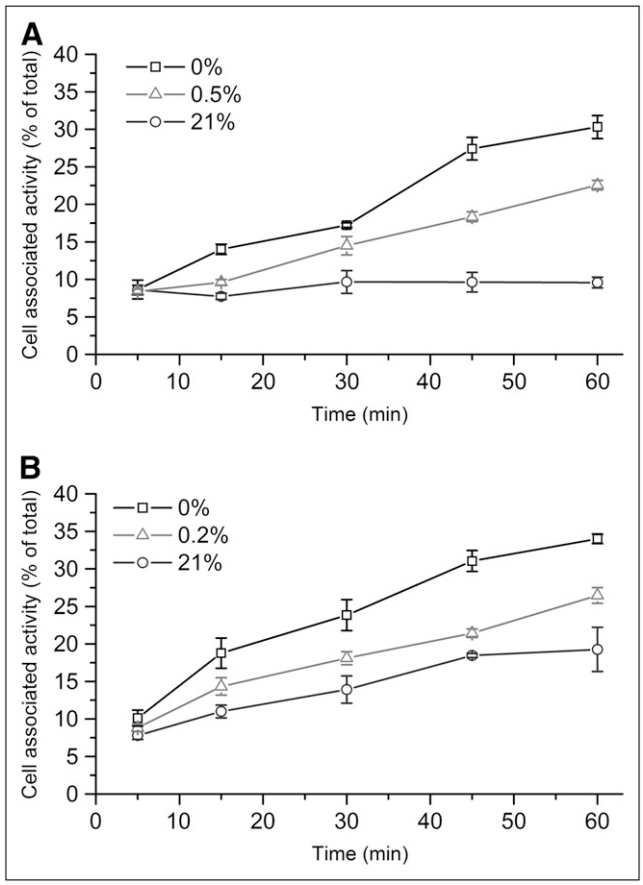

FIGURE 3. Percentages of uptake of ^{64}Cu-ATSE/A-G (A) and ^{64}Cu-ATSM (B) into HeLa cells over time at various oxygen concentrations. Errors, if not indicated, are within symbols.

For comparison, the uptake of ^{64}Cu-ATSM (the parent compound) was measured in the same cell line (Fig. 3B). O_2 concentration–dependent uptake was observed, as expected (*15,16*), but was higher than that of ^{64}Cu-ATSE/A-G under all conditions. The percentages of uptake at 60 min with 21%, 0.2% and 0% O_2 concentrations were 34.1%, 26.4%, and 19.3%, respectively. The differences in the percentages of uptake were found to be significant for both 21% and 0% O_2 ($P = 0.018$). However, under normoxic conditions, ^{64}Cu-ATSM uptake did not plateau after 30 min but continued to increase throughout the time course. The ratio of hypoxic uptake to normoxic uptake at 60 min was 1.4, considerably lower than that for ^{64}Cu-ATSE/A-G (especially considering that in the ^{64}Cu-ATSM experiment, a lower partial pressure of oxygen was used for the hypoxic samples). The hypoxic uptake values obtained for ^{64}Cu-ATSM were lower than those reported for the more widely used EMT6 (murine) cell line (*16*). Lewis et al. reported that uptake in this type of experiment is cell line dependent, and the lower level of uptake found in our study was thus ascribed to differences in the HeLa cell phenotype (*23*).

Serum Stability

Cold Cu-ATSE/A-G was incubated in rat serum, and the amount of the complex remaining in the solution was assessed with UV/visible-light spectroscopy at 30 and 60 min. After 30 min, 92% of the complex remained in the solution. At 60 min, the amount had decreased to 82%. With this method it was not possible to determine whether the tracer underwent decomposition or whether it became bound to serum proteins. The results are in accordance with those of a recent study of closely related lipophilic ^{64}Cu-ATSM derivatives in mouse serum, which showed that 20%–25% of the activity was protein bound after 60 min (*24*).

In Vivo PET with ^{64}Cu-ATSE/A-G

Two tumor-bearing rats were injected with 6 and 18 MBq of ^{64}Cu-ATSE/A-G on separate occasions. Although the new tracer was completely water soluble, ethanol (10%) was added for consistency with the ^{64}Cu-ATSM experiment. In both experiments, the observed biodistributions were similar. [**Fig. 4**] Figure 4 shows the reconstructed PET images for the 18-MBq experiment. The bladder and kidneys showed high uptake, suggesting that the primary excretion pathway for the water-soluble complex was renal. Significant retention in the tumor was observed, as was uptake in the liver and areas of the intestines. SUVs in the major organs were estimated for [**Fig. 5**] comparisons with ^{18}F-FDG and ^{64}Cu-ATSM (Fig. 5).

Comparison with ^{18}F-FDG

To test the possibility that ^{64}Cu-ATSE/A-G acts as a marker for glucose metabolism, we performed a control experiment with ^{18}F-FDG in the BDIX/P22 tumor model and with the same image acquisition and reconstruction protocols (Fig. 4). A strong correlation between the observed in vivo distributions of ^{64}Cu-ATSE/A-G and ^{18}F-FDG would indicate that the glucose subunit of the novel tracer controls its biodistribution pathway. Different patterns of uptake were immediately apparent on

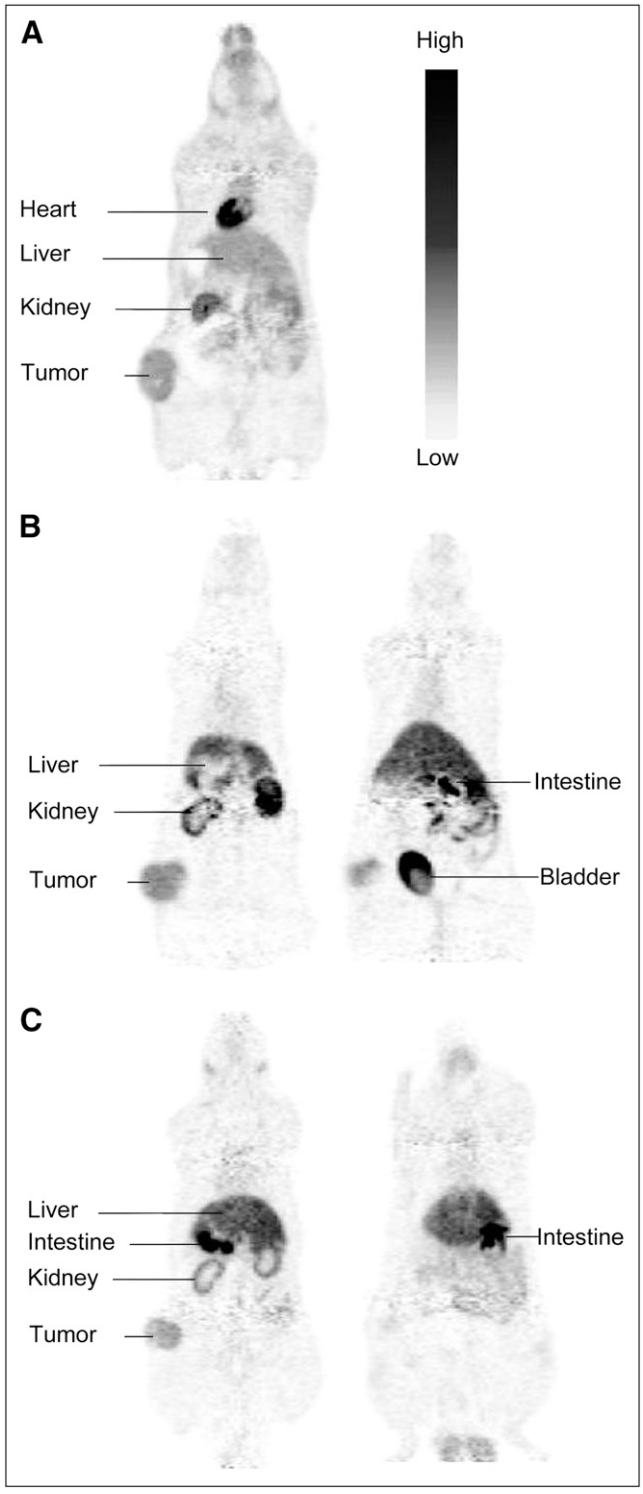

FIGURE 4. Coronal slices showing small-animal PET images obtained with ^{18}F-FDG (A), ^{64}Cu-ATSE/A-G (B), and ^{64}Cu-ATSM (C) injected into tail vein of P22 tumor–bearing rats. Slices shown in same panel were taken from one animal (superior to inferior).

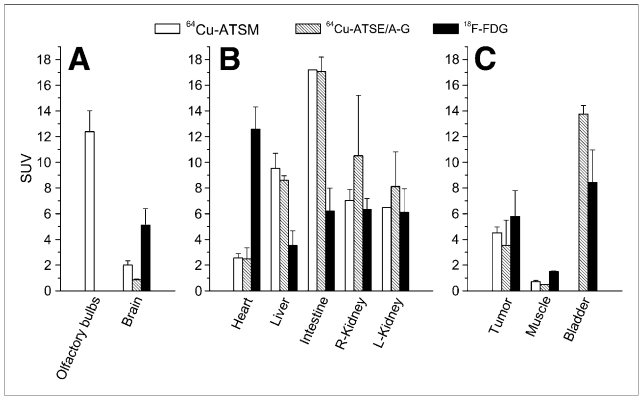

FIGURE 5. SUVs estimated from PET images obtained with ^{64}Cu-ATSM, ^{64}Cu-ATSE/A-G, and ^{18}F-FDG in BDIX rats with P22 carcinosarcomas (average of 2 imaging experiments). Results obtained at 18 min (A), 32 min (B), and 42 min (C) are shown. Error bars show SDs. Because of large variations between experiments, bladder SUV for ^{18}F-FDG was obtained from single PET image (error was estimated).

comparison of the ^{64}Cu-ATSE/A-G and ^{18}F-FDG images. In particular, the localization of ^{18}F-FDG in the brain and the heart was clearly visible. The SUVs in these organs were considerably higher for ^{18}F-FDG (5.1 and 12.6, respectively) than for ^{64}Cu-ATSE/A-G (0.9 and 2.5, respectively). Statistical analysis showed the differences to be significant ($P = 0.040$ for the brain and $P = 0.018$ for the heart). Liver uptake was also observed, but the SUV was significantly lower for ^{18}F-FDG than for ^{64}Cu-ATSE/A-G (3.5 and 8.6, respectively; $P = 0.027$). The tumor and kidneys also retained ^{18}F-FDG, but although the levels of uptake of ^{18}F-FDG appeared to be lower, the SUVs were not significantly different from those for ^{64}Cu-ATSE/A-G. The muscle uptake of ^{18}F-FDG was significantly higher than that of ^{64}Cu-ATSE/A-G (SUVs of 1.5 and 0.5, respectively; $P < 0.001$). The observed tumor/muscle SUV ratios were 3.9 for ^{18}F-FDG and 7.3 for ^{64}Cu-ATSE/A-G.

Comparison with ^{64}Cu-ATSM

A key aim of this work was to demonstrate that the in vivo distribution of ^{64}Cu-ATSM could be modified by derivatization. A control experiment with ^{64}Cu-ATSM was therefore performed with the BDIX/P22 tumor model and with the same image acquisition and reconstruction protocols (Fig. 4). ^{64}Cu-ATSM produced by the standard method from H_2-ATSM and ^{64}Cu-ATSM produced by transmetallation of Zn-ATSM showed identical biodistributions. Characteristic kidney, liver, and tumor retention was observed. ^{64}Cu-ATSM uptake in the brain was also discernible (SUV, 2.0), with very strong localization observed in the olfactory bulbs (SUV, 12.4). In contrast, ^{64}Cu-ATSE/A-G uptake in the brain was minimal (SUV, 0.9; in a comparison with ^{64}Cu-ATSM, the P value was 0.042), and the olfactory bulbs could not be delineated. Also, unlike ^{64}Cu-ATSE/A-G, activity in the bladder due to ^{64}Cu-ATSM was too low for this organ to be delineated.

DISCUSSION

The results of the in vitro study demonstrated that ^{64}Cu-ATSE/A-G possesses oxygen-dependent uptake properties similar to those of ^{64}Cu-ATSM. Thus, conjugation of the exocyclic nitrogen atom of the Cu-bis(thiosemicarbazonato) complex does not negate its hypoxia selectivity. In fact, although the hydrophilic glucose unit did appear to reduce overall uptake at all oxygen concentrations (perhaps because of a reduced rate of diffusion through the cell membrane), in HeLa cells the hypoxia selectivity of ^{64}Cu-ATSE/A-G was improved. The lower level of normoxic uptake shown by ^{64}Cu-ATSE/A-G led to a far higher ratio of hypoxic uptake to normoxic uptake for this tracer than for ^{64}Cu-ATSM.

One problem limiting the clinical use of ^{64}Cu-ATSM is its high level of liver uptake (*25*). The complex is highly lipophilic (water-to-octanol partition coefficient [log$P$] = 1.5) and hence has extremely low solubility in water. Previous work suggested that ^{64}Cu-ATSM does not circulate as a molecular species but is more likely to be bound to lipophilic sites in proteins or membranes. The related tracer ^{64}Cu-ATSE showed 20% protein-associated radioactivity when tested after dilution in serum (*26*). These properties also explain why the primary excretion pathway for ^{64}Cu-ATSM is hepatointestinal, as observed in our PET study. Small lipophilic molecules are also able to cross the blood–brain barrier (*27*), leading to the observed brain uptake of the complex. The production of ^{64}Cu-ATSM by transmetallation of Zn-ATSM rather than by the standard method resulted in no discernible difference in the observed in vivo distribution.

A serum stability test with cold Cu-ATSE/A-G produced results similar to those observed previously for ^{64}Cu-ATSM, with 18% of the tracer being lost from the solution after 1 h. This finding was somewhat surprising, as Cu-ATSE/A-G is highly water soluble (log$P = 0.5$) because of the hydrophilic glucose unit and was expected to have a low affinity for serum proteins (*19*). It is possible that Cu-ATSE/A-G acts as an amphiphile and that the lipophilic Cu-bis(thiosemicarbazonato) unit binds to serum proteins with an affinity similar to Cu-ATSE. Alternatively, the complex could undergo hydrolysis of the linkage between the Cu-bis(thiosemicarbazonato) and glucose units, resulting in decomposition and release of the copper(II) ion.

The high levels of kidney and bladder accumulation observed in the in vivo PET studies with ^{64}Cu-ATSE/A-G indicated that the renal pathway functioned as a route of excretion for this tracer (^{64}Cu-ATSM accumulated in the kidneys but was not excreted into the bladder). The brain uptake of ^{64}Cu-ATSE/A-G was also very low, consistent with the low log$P$ of the complex. These results imply that the glucose subunit exerts some control over the biodis-

tribution of the ^{64}Cu complex, because it is directed to target organs for excretion of hydrophilic species and is excluded from compartments accessible only to lipophilic (or actively transported) species. Our PET study was not designed to test the hypoxia selectivity of ^{64}Cu-ATSE/A-G. It was intended as an initial qualitative study of biodistribution, the tumor model used was not thought to be hypoxic, and no attempt was made to measure tumor oxygenation.

^{18}F-FDG, a marker for glucose metabolism, is by far the most studied PET tracer, is in routine clinical use, and is produced commercially (*28*). Recently, much attention has been directed toward producing analogs of ^{18}F-FDG that incorporate a metallic radionuclide (particularly ^{99m}Tc for SPECT) instead of ^{18}F (*29–31*). None of these metallo-glucose conjugates has yet shown the ability to map glucose metabolism. This result is perhaps not surprising, because the addition of a bulky metal-bearing group to a small molecule such as glucose will lead to gross changes in its biochemical properties. In our PET study, ^{64}Cu-ATSE/A-G and ^{18}F-FDG showed obviously divergent biodistributions (particularly in the brain and the heart); this result seems to confirm the notion that ^{64}Cu-ATSE/A-G does not participate in glucose-specific transport or metabolism.

CONCLUSION

We have demonstrated that conjugation of the copper-bis(thiosemicarbazonato) complex at the exocyclic nitrogen with glucose leads to a modified biodistribution profile, with the excretion pathway being switched from primarily hepatointestinal (for ^{64}Cu-ATSM) to partially renal (for ^{64}Cu-ATSE/A-G). We have also confirmed that ^{64}Cu-ATSE/A-G retains hypoxia selectivity in vitro, with an improved ratio of hypoxic uptake to normoxic uptake, when compared with ^{64}Cu-ATSM. A quantitative PET study with a hypoxic tumor model is required to determine whether these characteristics are replicated in vivo. Thus, we have obtained proof of the concept that the biodistribution of ^{64}Cu-ATSM can be modified by derivatization without negating its favorable tumor-targeting properties and hypoxia selectivity.

ACKNOWLEDGMENTS

We are grateful to Dr. Sally Hill and Dr. Katie Wood for helpful discussions. We thank Peter Wardman for resources at the Gray Cancer Institute in Northwood. We thank Vivien Prise and Ian Wilson for implanting tumors; Anne Clark, Ann Marriot, and Valerie Edwards for the welfare and care of the animals; and Dr. Katrin Probst and Oksana Golovko for their assistance with radio-HLPC. The work was funded by CRUK (C5255/A8591), Siemens Molecular Imaging Ltd., and the U.K. Department of Trade and Industry. We thank GlaxoSmithKline for funding as well as Merton College and the U.K. Engineering and Physical Sciences Research Council for a studentship.

REFERENCES

1. Hedley D, Pintilie M, Woo J, et al. Carbonic anhydrase IX expression, hypoxia, and prognosis in patients with uterine cervical carcinomas. *Clin Cancer Res.* 2003;9:5666–5674.
2. Nordsmark M, Overgaard J. A confirmatory prognostic study on oxygenation status and loco-regional control in advanced head and neck squamous cell carcinoma treated by radiation therapy. *Radiother Oncol.* 2000;57:39–43.
3. Nordsmark M, Overgaard M, Overgaard J. Pretreatment oxygenation predicts radiation response in advanced squamous cell carcinoma of the head and neck. *Radiother Oncol.* 1996;41:31–39.
4. Pugh CW, Ratcliffe PJ. Regulation of angiogenesis by hypoxia: role of the HIF system. *Nat Med.* 2003;9:677–684.
5. Dachs GU, Tozer GM. Hypoxia modulated gene expression: angiogenesis, metastasis and therapeutic exploitation. *Eur J Cancer.* 2000;36:1649–1660.
6. Isa AY, Ward TH, West CML, Slevin NJ, Homer JJ. Hypoxia in head and neck cancer. *Br J Radiol.* 2006;79:791–798.
7. Dubois L, Landuyt W, Haustermans K, et al. Evaluation of hypoxia in an experimental rat tumor model by [F-18]fluoromisonidazole PET and immunohistochemistry. *Br J Cancer.* 2004;91:1947–1954.
8. Troost EGC, Bussink J, Laverman P, et al. Comparison of ^{18}F-MISO autoradiography with immunohistochemistry after modification of hypoxia in human glioma and squamous cell xenografts. *Radiother Oncol.* 2006;78(suppl):S33–S34.
9. Troost EGC, Laverman P, Kaanders JH, et al. Imaging hypoxia after oxygenation-modification: comparing [^{18}F]FMISO autoradiography with pimonidazole immunohistochemistry in human xenograft tumors. *Radiother Oncol.* 2006;80:157–164.
10. Fujibayashi Y, Taniuchi H, Yonekura Y, Ohtani H, Konishi J, Yokoyama A. Copper-62-ATSM: a new hypoxia imaging agent with high membrane permeability and low redox potential. *J Nucl Med.* 1997;38:1155–1160.
11. Lewis JS, McCarthy DW, McCarthy TJ, Fujibayashi Y, Welch MJ. Evaluation of Cu-64-ATSM in vitro and in vivo in a hypoxic tumor model. *J Nucl Med.* 1999;40:177–183.
12. Dehdashti F, Grigsby PW, Mintun MA, Lewis JS, Siegel BA, Welch MJ. Assessing tumor hypoxia in cervical cancer by positron emission tomography with Cu-60-ATSM: relationship to therapeutic response—a preliminary report. *Int J Radiat Oncol Biol Phys.* 2003;55:1233–1238.
13. Dehdashti F, Mintun MA, Lewis JS, et al. In vivo assessment of tumor hypoxia in lung cancer with ^{60}Cu-ATSM. *Eur J Nucl Med Mol Imaging.* 2003;30:844–850.
14. Dehdashti F, Grigsby PW, Lewis JS, Laforest R, Siegel BA, Welch MJ. Assessing tumor hypoxia in cervical cancer by PET with Cu-60-labeled diacetyl-bis(*N*-4-methylthiosemicarbazone). *J Nucl Med.* 2008;49:201–205.
15. Vavere AL, Lewis JS. Cu-ATSM: a radiopharmaceutical for the PET imaging of hypoxia. *Dalton Trans.* 2007;November:4893–4902.
16. Dearling JLJ, Lewis JS, McCarthy DW, Welch MJ, Blower PJ. Redox-active metal complexes for imaging hypoxic tissues: structure-activity relationships in copper(II) bis(thiosemicarbazone) complexes. *Chem Commun.* 1998;November:2531–2532.
17. Dearling JLJ, Lewis JS, Muller GED, Welch MJ, Blower PJ. Copper bis(thiosemicarbazone) complexes as hypoxia imaging agents: structure-activity relationships. *J Biol Inorg Chem.* 2002;7:249–259.
18. Christlieb M, Dilworth JR. Ligands for molecular imaging: the synthesis of bis(thiosemicarbazone) ligands. *Chemistry.* 2006;12:6194–6206.
19. Holland JP, Aigbirhio FI, Betts HM, et al. Functionalized bis(thiosemicarbazonato) complexes of zinc and copper: synthetic platforms toward site-specific radiopharmaceuticals. *Inorg Chem.* 2007;46:465–485.
20. Cowley AR, Davis J, Dilworth JR, et al. Fluorescence studies of the intra-cellular distribution of zinc bis(thiosemicarbazone) complexes in human cancer cells. *Chem Commun.* 2005;February:845–847.
21. Sensky PL, Prise VE, Tozer GM, Shaffi KM, Hirst DG. Resistance to flow through tissue-isolated transplanted rat tumors located in two different sites. *Br J Cancer.* 1993;67:1337–1341.
22. Tai YC, Ruangma A, Rowland D, et al. Performance evaluation of the microPET Focus: a third-generation microPET scanner dedicated to animal imaging. *J Nucl Med.* 2005;46:455–463.
23. Burgman P, O'Donoghue JA, Lewis JS, Welch MJ, Humm JL, Ling CC. Cell line-dependent differences in uptake and retention of the hypoxia-selective nuclear imaging agent Cu-ATSM. *Nucl Med Biol.* 2005;32:623–630.
24. Bonnitcha PD, Vavere AL, Lewis JS, Dilworth JR. In vitro and in vivo evaluation of bifunctional bisthiosemicarbazone ^{64}Cu-complexes for the positron emission tomography imaging of hypoxia. *J Med Chem.* 2008;51:2985–2991.

25. Laforest R, Dehdashti F, Lewis JS, Schwarz SW. Dosimetry of Cu-60/61/62/64-ATSM: a hypoxia imaging agent for PET. *Eur J Nucl Med Mol Imaging.* 2005;32:764–770.
26. McQuade P, Martin KE, Castle TC, et al. Investigation into Cu-64-labeled bis(selenosemicarbazone) and bis(thiosemicarbazone) complexes as hypoxia imaging agents. *Nucl Med Biol.* 2005;32:147–156.
27. Pardridge WM. Transport of small molecules through the blood-brain-barrier: biology and methodology. *Adv Drug Deliv Rev.* 1995;15:5–36.
28. Gambhir SS, Czernin J, Schwimmer J, Silverman DHS, Coleman RE, Phelps ME. A tabulated summary of the FDG PET literature. *J Nucl Med.* 2001;42(5 suppl):1S–93S.
29. Bayly SR, Fisher CL, Storr T, Adam MJ, Orvig C. Carbohydrate conjugates for molecular imaging and radiotherapy: Tc-99m(I) and Re-186(I) tricarbonyl complexes of N-(2′-hydroxybenzyl)-2-amino-2-deoxy-D-glucose. *Bioconjug Chem.* 2004;15:923–926.
30. Schibli R, Dumas C, Petrig J, et al. Synthesis and in vitro characterization of organometallic rhenium and technetium glucose complexes against Glut 1 and hexokinase. *Bioconjug Chem.* 2005;16:105–112.
31. Ferreira CL, Bayly SR, Green DE, et al. Carbohydrate-appended 3-hydroxy-4-pyridinone complexes of the $[M(CO)_3]^+$ core (M = Re, ^{99m}Tc, ^{186}Re). *Bioconjug Chem.* 2006;17:1321–1329.

jnm054015-pe ■ 10/10/08